ADVANCED MATERIALS

Supporting Information

for *Adv. Mater.*, DOI 10.1002/adma.202302237

Large-Scale Molecular Dynamics Elucidates the Mechanics of Reinforcement in Graphene-Based Composites

*James L. Suter, Maxime Vassaux and Peter V. Coveney**

Supporting Information: Large-scale molecular dynamics elucidates the mechanics of reinforcement in graphene-based composites

James L. Suter 0000-0002-0149-7974,[†] Maxime Vassaux 0000-0003-2975-0625,[‡] and Peter V. Coveney 0000-0002-8787-7256[*,†,¶,§]

[†]*Centre for Computational Science - University College London, 20 Gordon Street, London, WC1H 0AJ, United Kingdom*

[‡]*Institute of Physics Rennes, CNRS, IPR- UMR 6251, F-35000*

[¶]*Advanced Research Computing Centre, University College London, London, WC1E 6BT, United Kingdom*

[§]*Computational Science Laboratory, Institute for Informatics, Faculty of Science, University of Amsterdam, 1098XH, The Netherlands*

E-mail: p.v.coveney@ucl.ac.uk

In this Supporting Information (SI), we report in detail the graphene and graphene-oxide PVA simulation systems used in this study.

S1 MD production simulations

In Table S1, we list the size and total number of atoms of the graphene and graphene oxide systems. This size of simulation, and the number of simulations, is unprecedented for

Table S1: The Graphene/graphene-oxide PVA models studied in this paper. For each system, 7 replica simulations with different initial seeds to the velocities randomly drawn from a Maxwell-Boltzmann distribution. Lattice dimensions are given for the system at 200K with zero strain applied, averaged over the 7 replicas in each ensemble.

		lattice dimensions				
flake	flake size (Å)	x (Å)	y (Å)	z (Å)	initial x (Å)	number of atoms
graphene	2000	21775.4	184.6	91.4	22000	29676152
graphene	500	5895.7	186.2	87.8	6000	8076044
graphene	400	4722.5	187.4	90.0	4800	6460844
graphene	300	3539.9	188.5	91.4	3600	4845644
graphene	200	2347.7	188.1	91.3	2400	3230444
graphene	100	1166.5	188.6	91.4	1200	1615244
GO	2000	22533.1	190.8	93.5	22000	30126733
GO	500	6088.9	191.4	91.2	6000	8189030
GO	400	4890.1	191.6	91.5	4800	6550954
GO	300	3643.5	188.8	89.9	3600	4913168
GO	200	2435.1	189.1	89.5	2400	3275451
GO	100	1211.0	188.4	89.3	1200	1637824

studying the behaviour of graphene / graphene-oxide systems.

We generate the oxidised graphene structures using the procedure described in our previous publication[1–3]. To summarise this procedure, the algorithm generates graphene oxide nanostructures for atomistic simulation based on theoretical and experimental evidence[2], which improves upon the current standard approach of an uncorrelated random distribution of oxidised functional groups, based on the Lerf-Klinowski model[4]. Our algorithm uses the quantum mechanical (QM) simulations of Yang *et al.*[5], which studied the reactivity of various reactive intermediate structures and showed that graphene oxidation is overwhelmingly favoured adjacent to already oxidised carbons. As can be seen in Figure 1 of the main paper, our algorithm creates atomistic structures of GO that successfully recreate the two-phase nature of oxidised and unoxidised graphene domains observed in microscopy experiments, and is necessary to reproduce GO assembly due to the self-attraction of graphene domains.

Here we are only considering oxidation on the basal surface consisting of hydroxyl and epoxy groups. To oxidise the edge groups, we selected 1/4 of the edge carbon edge atoms and these were converted to (protonated) carboxylic acid groups.

S2 Ensemble generation and averaging

This study was made possible by using the software provided within the VECMA toolkit `https://www.vecma-toolkit.eu/`. We especially relied on the EasyVVUQ software `https://easyvvuq.readthedocs.io/`[6]. This software allows us to efficiently sample over a defined input parameter space, and automatic collation of ensemble results.

These simulations have chaotic dynamics and are thus sensitive to their initial conditions. For all systems we therefore simulated ensembles to acquire reproducible results. Each replica in the ensemble has unique, uncorrelated velocities drawn from a Maxwell-Boltzmann distribution.

An ensemble of 14 replicas was studied to identify the optimal number of replicas required. We used as our test system the 300nm graphene flake system. This size of flake is at the point of highest increase in the Young's modulus as function of flake size (Main Paper Figure 2) and therefore expected to have a large variation in the predicted Young's modulus. A bootstrap with replacement was performed on this sample to quantify the confidence in the results that were derived. 'Resamples' from the original 14 simulations were taken, at random, with replacement, of size N. In Figure S1, we show the 95% confidence as function of ensemble size calculated by a bootstrap method. We decided that 7 is a reasonable ensemble size at which there are diminishing returns with respect to the average Young's modulus.

S3 Graphene-oxide structure

In Figure S2, we show a graphene-oxide chemical structure diagram illustrating the different chemical oxidative groups present on the basal surface and the edge of the graphene flake. These include hydroxyl and epoxy groups on the basal surface, and an equal number of protonated carboxylic acid groups and hydroxyl groups on the edge of the flake.

Detailed visualisations of the graphene-oxide surface are shown in Figure S3, where the different oxidative species and the oxidised and unoxidised domains can clearly be seen. The

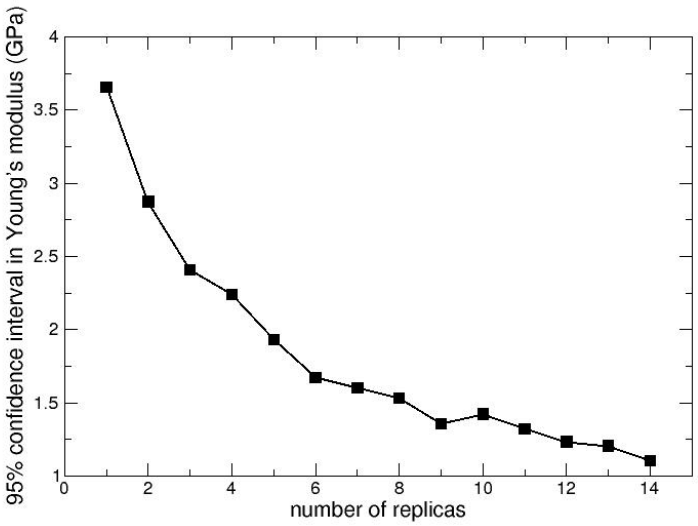

Figure S1: A bootstrap with replacement study on the 300nm graphene system with varying the resample size showing the variation of the 95% confidence interval of the computed Young's modulus, calculated by a bootstrap method. Here, one can see 7 is a reasonable point at which there are diminishing returns.

OPLS forcefield parameters for GO are given in Section S7.

S4 Graphene/GO - polymer interface

We have analysed the interfacial behaviour between the graphene / GO surface and the PVA polymer. In Figure S4a, we show the atomic density profile perpendicular to the graphene surface, averaged over the final 0.1ns of our simulation at 300K. To do so, we calculated the average z coordinate of the graphene sheet (which lies in the xy plane) for each point on a grid in the xy plane with spacing of 3.5 Å to create a graphene height-function. The atomic density of the polymer was calculated within this xy voxel as a function of difference in z coordinate with the average graphene z position within the grid. Densities were not calculated if there were no graphene atoms were within the grid, thereby removing contributions from polymer to the side of the graphene flake. The densities were summed to create Figure S4. This method removes the broadening effects of flake undulations if it is

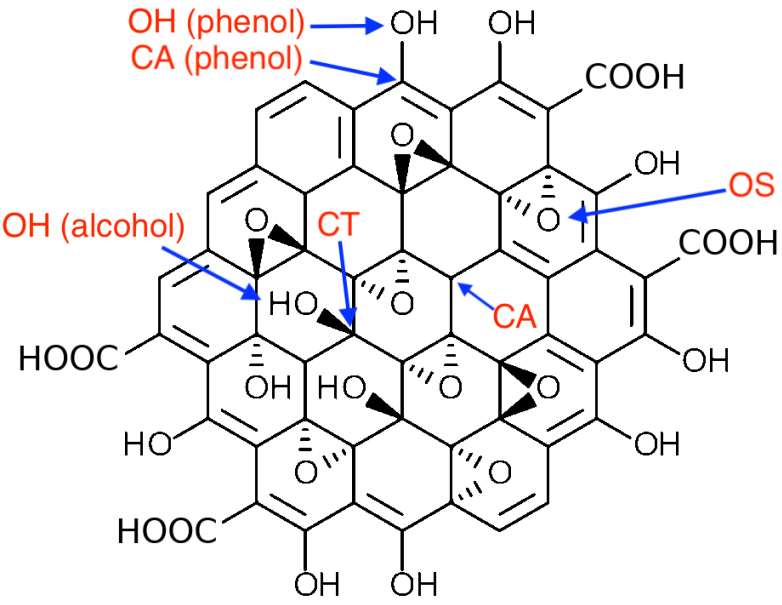

Figure S2: Chemical structure of graphene-oxide. Our GO models have epoxy and hydroxyl groups on the basal surface, and carboxylic acid and hydroxyl groups on the edge. Indicated in red are OPLS atom types as found in Table S3.

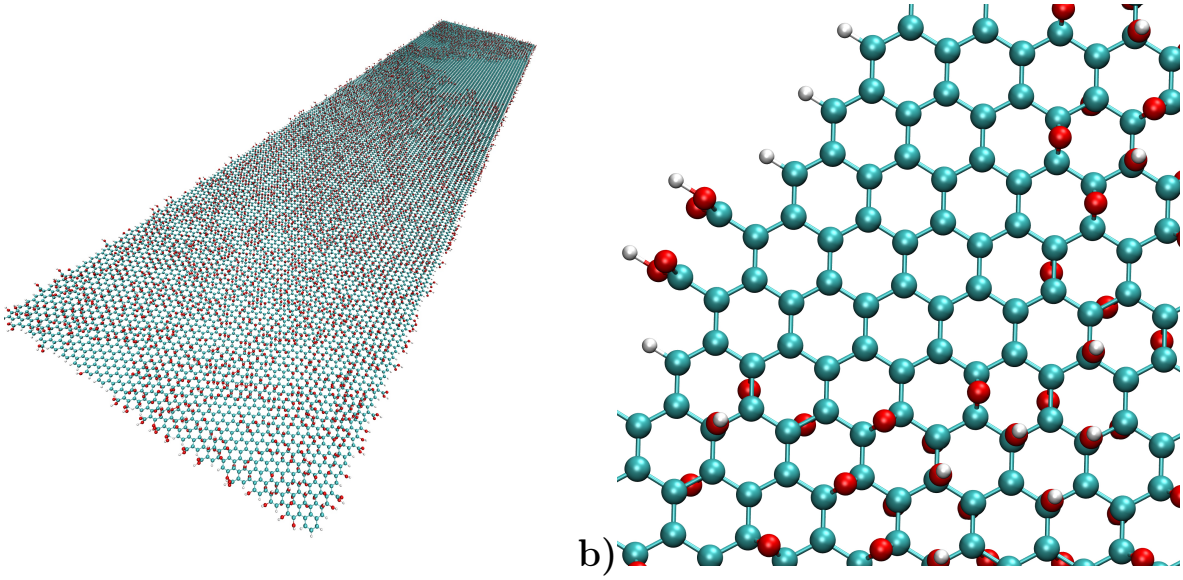

Figure S3: Visualisations of the GO flakes used in this study. a) Visualisation of a GO sheet of 100nm length and 10nm width. The C:O ratio is 2.5, indicating a large degree of oxidation. The model contains domains of both oxidised and unoxidised regions. b) A close up view of the edge of the GO flake. Hydroxyl groups and epoxy groups are on the basal surface, above and below the GO surface. Carboxyl acids and hydroxyl groups are on the edge. It can clearly be seen that there is a region of unoxidised graphene-like carbons bordering a oxidised region. Atom colours are as follows: green are carbon atoms, red are oxygen atoms and white are hydrogen atoms.

simply assumed that the graphene flake lies flat in the xy plane and the atomic density can be computed purely from the polymer z coordinates. The density profiles are normalised to 1 if the polymer was randomly distributed.

Figure S4a shows the polymer carbon backbone atom have maximum density at approximately 3.8 Å above and below the graphene surface. The polymer forms a layer on the surface of the graphene, with a second layer peak at approximately 8.5 Å from the graphene surface. Above 15 Å above and below the surface, the polymer has predominately returned to bulk behaviour, with approximately constant density.

In Figure S4b, we show the density profile of the undulatory graphene flake compared to the planar flake. We see very little difference between the profiles, with the only variation is a slight broadening of the first peak of polymer molecules. Note, this could be due to the difficulties in correcting for larger undulations in the flake when calculating the density profile. We also show the integral of the density profile, which clearly shows the amount of polymer atoms in the first peak to be identical whether the flake is undulatory or planar. This indicates that the interfacial bonding between the flake and the polymer is unaffected by the undulations in the flake surface.

For GO, the position of the GO flake within the grid is computed from the average position of the sp^2 and sp^3 carbon atoms in the GO flake. In Figure S4c, we see the carbon density is now further away from the GO surface, with the hydroxyl oxygen and hydrogen atoms forming a broad peak between approximately 3Å and 5 Å, indicating the large amount of hydrogen bonding between the epoxy and hydroxyl groups on the GO basal surface and the hydroxyl group of the polymer.

To further investigate the interaction between the GO surface and polymer hydroxyl groups, we have computed the radial distribution functions between the hydroxyl groups on the GO surface and the polymer molecules. In Figure S5, we see that the polymer hydroxyl hydrogen atoms form hydrogen bonds with the epoxy groups on the GO surface (green line) and the polymer hydroxyl oxygen atoms form hydrogen bonds with the hydroxyl hydrogen

atoms on the GO surface (red line). Integrating the radial distribution function up to 3.8 Å, we find 2 hydrogen atoms for each GO epoxy oxygen atom, and 1 oxygen atom for each GO hydroxyl hydrogen, indicating that all GO functional oxidative groups are participating in their maximum hydrogen bonding capability with the surrounding polymer.

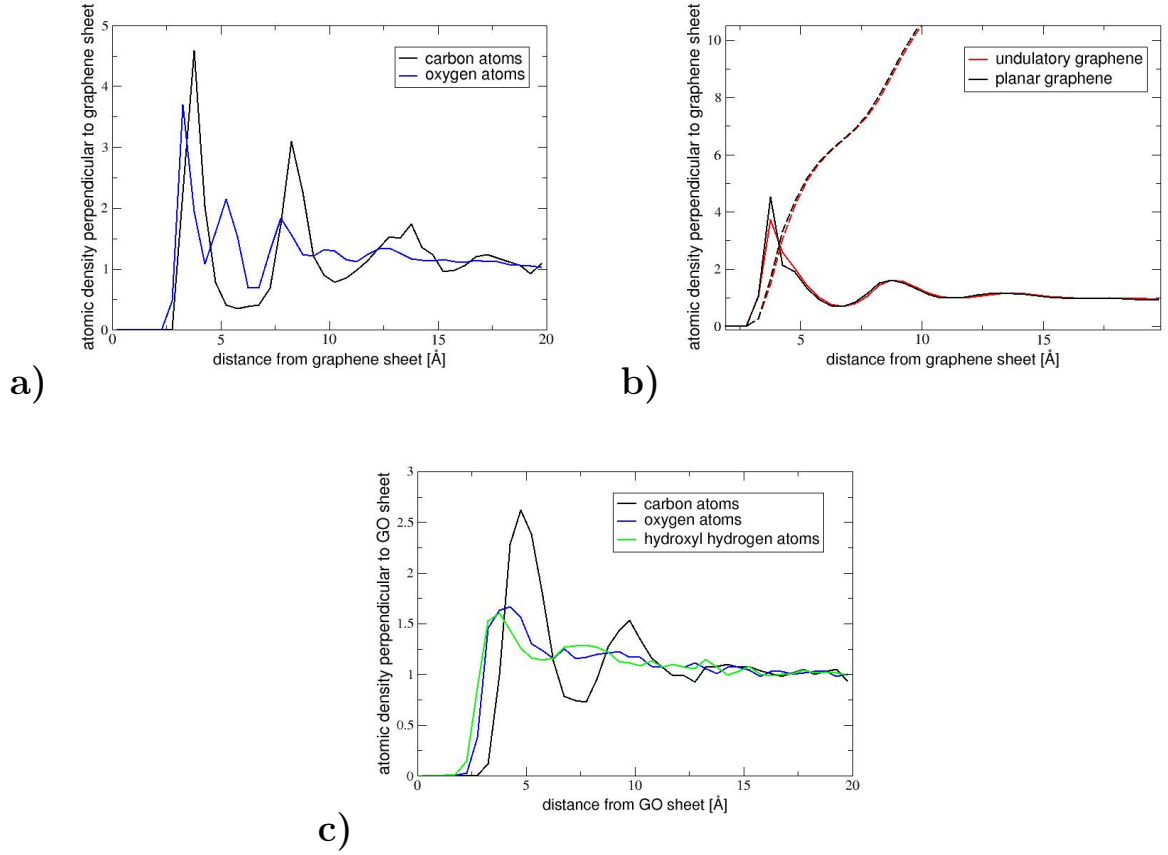

Figure S4: a) Atomic density profiles for the polymer atoms perpendicular to the graphene surface. b) Comparison between the density profile for the polymer carbon atoms perpendicular to the surface for the planar and undulatory graphene surface. The integral of the density profile is shown by the dotted lines. c) Atomic density profiles for the polymer atoms perpendicular to the GO surface.

S5 Flake compression in the transverse direction

To analyse whether any buckling in the transverse direction is occurring with strain, we have computed the density profiles at zero strain and at 0.2% strain for a replica of the 2000nm

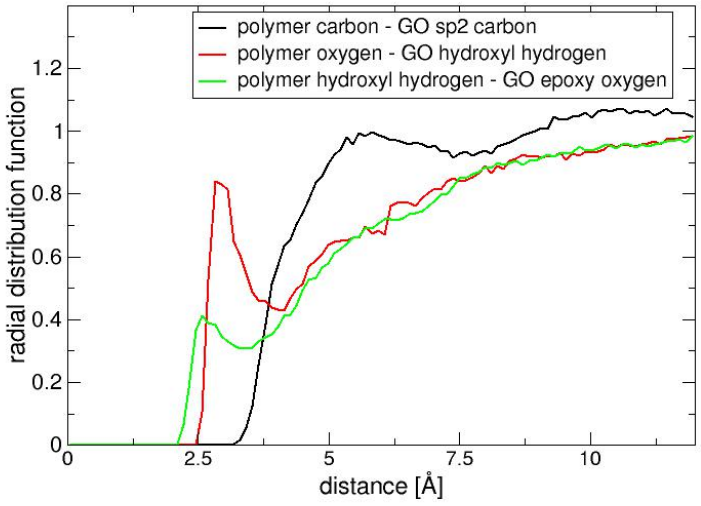

Figure S5: Radial distribution functions between hydroxyl atoms on the GO basal surface and the polymer. Also shown is the radial distribution function between sp^2 carbon atoms in GO and backbone carbon atoms of PVA.

graphene system. As shown in Figure S6, we see no change in the density profile, indicating that there is no change in the interfacial behaviour.

To check whether any buckling is occurring in the transverse direction (y direction in our simulation set-up), we have computed the Fourier transform of the height function of the graphene sheet in the y direction. We see very little difference in the amplitude of the undulations, as shown in Figure S7, indicating no buckling has occurred. There is no increase in the low wavenumber, long wavelength modes associated with buckling.

We can examine the compressive strain within the flake in the y direction, transverse to the direction of strain, that occurs due to Poisson contraction. Using the same methodology as Figure 3 in the main paper for strain in the axial direction, we computed the change in bond length for bonds that predominantly point in the y direction when the composite is at a strain of 0.2%. In Figure S8, we see that there is no shear-lag behaviour, as shown in the axial direction. This is to be expected as the flake is only 10nm wide. Instead we see a fluctuating pattern of bond compression across the flake. There is very little difference

between the compression in the y direction and compression computed using the full bond length, indicating that all the compression is in-plane and there is very little out-of-plane displacement associated with the Poisson compression.

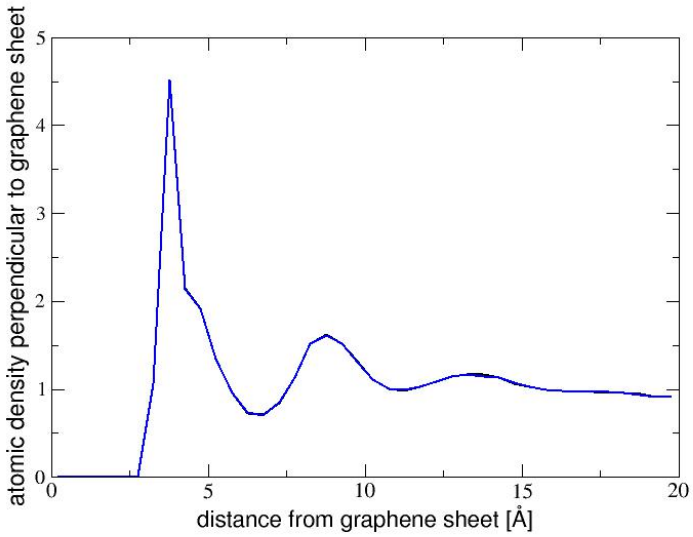

Figure S6: Atomic density profile of the carbon backbone atoms perpendicular to the graphene surface at zero strain (black) and at 0.2% strain blue for a 2000nm long graphene system. The two density profiles are virtually identical, indicating that no change in the interfacial behaviour.

S6 Stress-strain profiles

In Figures S9 and S10, we show the stress strain profiles from 0 to 0.2% for the graphene and GO systems respectively, ranging from 100nm to 2000nm in length. The gradient of the stress-strain profiles was used to calculate the Young's modulus of the composites. For the 100nm-500nm systems, we have displayed the rolling average over 0.01% to aid visualisation by removing fluctuations. For the 2000nm, the fluctuations are relatively small and no averaging was needed.

We can see the stress-strain profiles are approximately linear, indicating that we are in the linear regime and it is appropriate to use the gradient to determine the Young's modulus

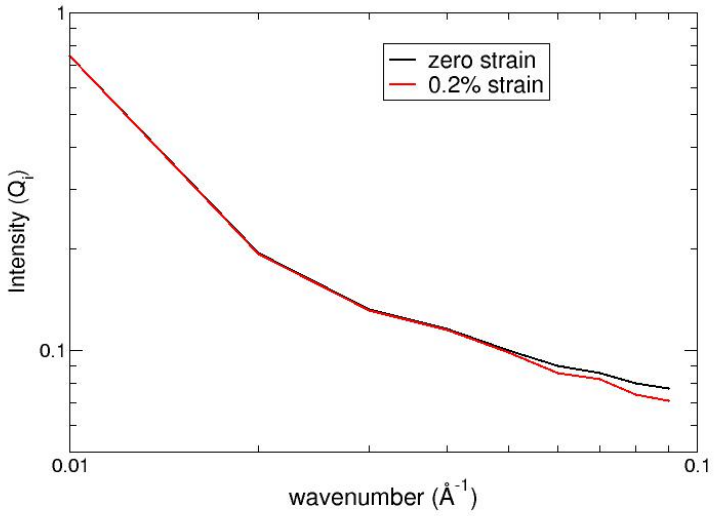

Figure S7: A Fourier transform of the height of the undulatory graphene (black) and planar graphene (red). The undulatory graphene shows much greater intensity for both long and short wavelength undulations.

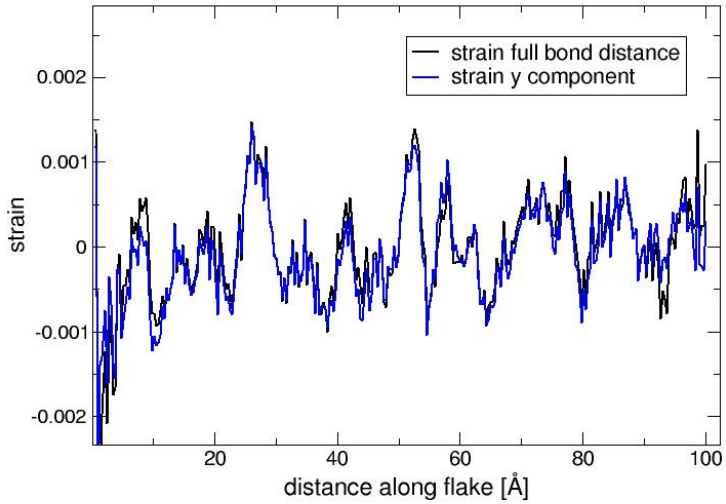

Figure S8: The strain field within the flake is calculated within the graphene flake by considering changes in the bond distances between the non-strained flake and the strained atom positions. Only bonds which are predominantly in the y direction are considered. Differences in bond distance (r'-r) and the difference in the y component of the bond are calculated, and converted to a local bond strain by dividing by r and the y component of the zero strain bond respectively. The figure shows the resulting strain field within the 2000nm graphene flake, with an imposed strain of 0.2% on the composite.

of the composites.

S7 Force-field parameters

The polymer, graphene and graphene-oxide in our study used the standard OPLS-AA force-field terms. A full list of forcefield terms for OPLS-AA is available as part of our GO atomic model builder[2], at
https://github.com/velocirobbie/make-graphitics/blob/master/makegraphitics/params/oplsaa.prm.
A list of the atom types used in this study, along with their non-bonded parameters, is given in Table S2 and S3 for PVA and graphene/GO respectively. The different atom types are indicated in Figure S2. Atom types can have atoms of different partial charge, depending on the atom types it is bound to. Bonds are calculated using a harmonic potential:

$$E = K(r - r_0)^2 \tag{1}$$

Where K is the spring constant and r_0 the equilibrium distance. Table S4 and S5 give these parameters for PVA and graphene/GO respectively.

Angles are calculated using a harmonic potential:

$$E = K(\theta - \theta_0)^2 \tag{2}$$

where θ_0 is the equilibrium value of the angle, and K is a prefactor. Table S6 and S7 give these parameters for PVA and graphene/GO respectively.

Dihedral energies are calculated using the following equation:

$$\begin{aligned} E = &\frac{1}{2}K_1[1 + \cos(\phi)] + \frac{1}{2}K_2[1 - \cos(2\phi)] + \\ &\frac{1}{2}K_3[1 + \cos(3\phi)] + \frac{1}{2}K_4[1 - \cos(4\phi)] \end{aligned} \tag{3}$$

K_1, K_2, K_3 and K_4 are given in Tables S8 and S9 for PVA and graphene/GO respectively.

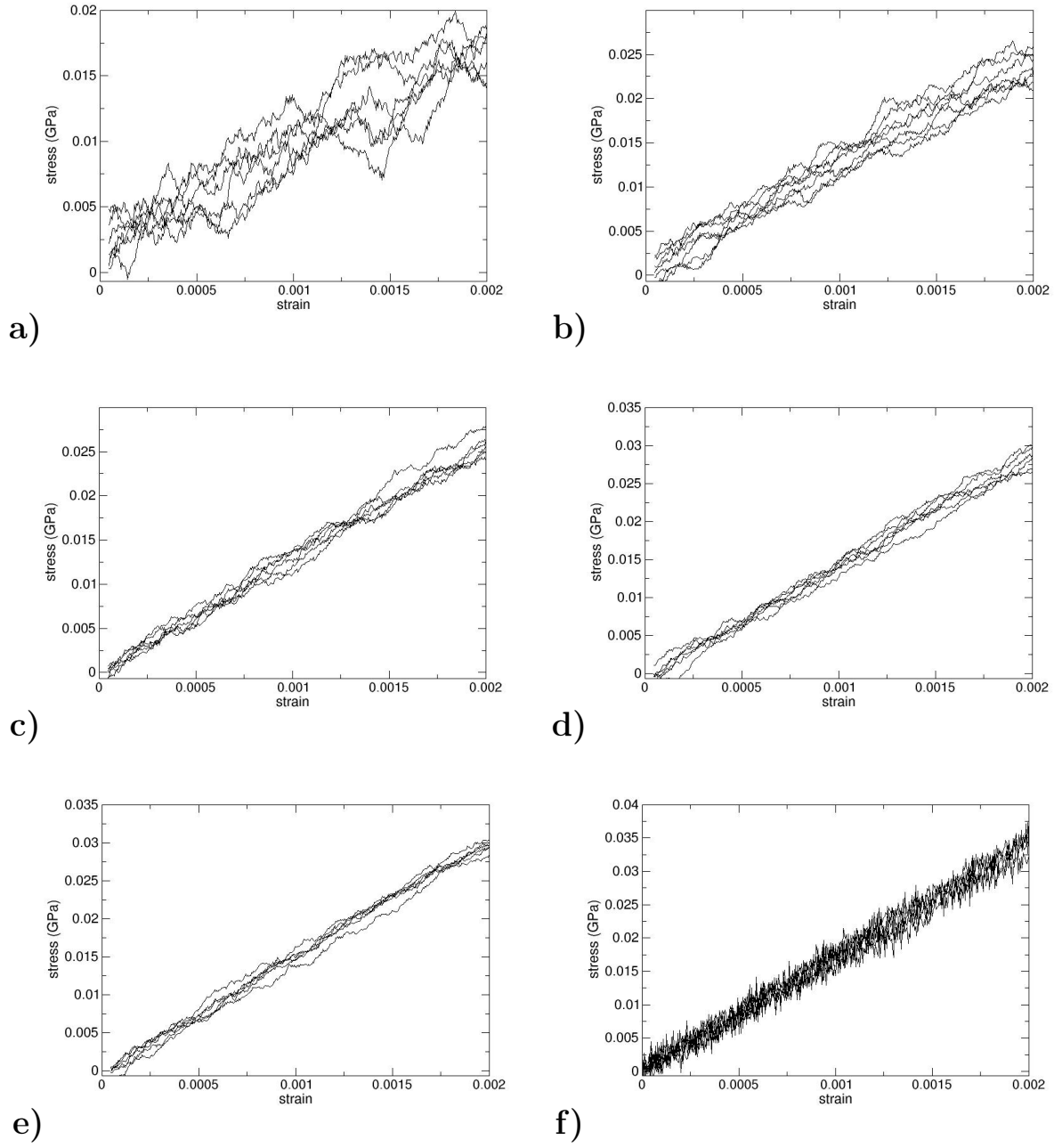

Figure S9: stress-strain profiles for the each of the replicas of the graphene systems listed in S1.

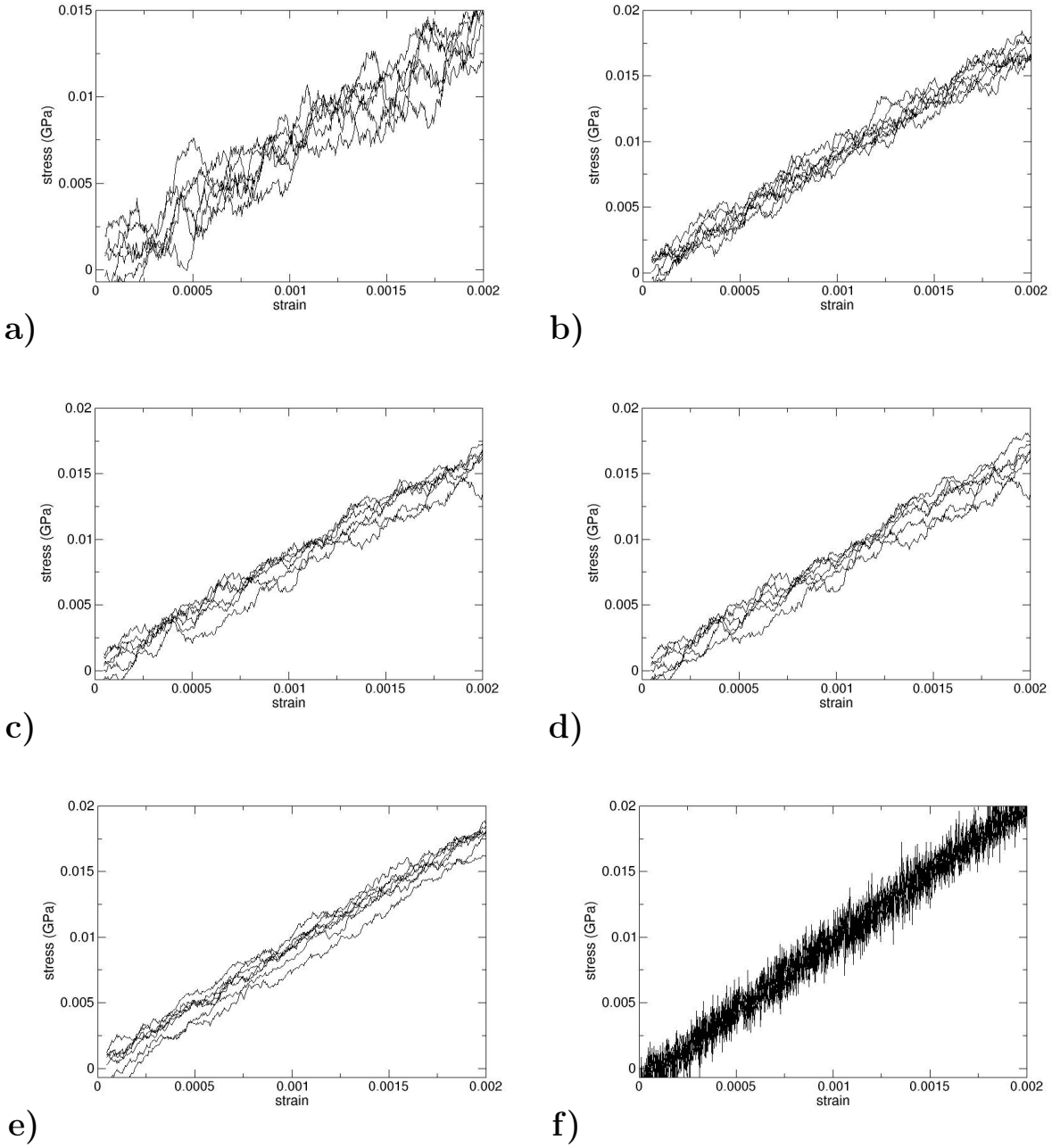

Figure S10: stress-strain profiles for the GO systems listed in S1.

Impropers for graphene/GO are calculated using an harmonic potential. See https://docs.lammps.org/improper_harmonic.html for a definition of the 4 atoms involved in a improper interaction.

$$E = K(\chi - \chi_0)^2 \tag{4}$$

. K and χ_0 (the equilibrium angle) is given in Table S10.

Table S2: OPLS parameters: PVA atom types

OPLS atom type	Description	Lennard-Jones parameters		Atomic charges
		ϵ (Kcal mol^{-1})	σ (Å)	
CT	Alkane CH3-	0.066	3.5	-0.18
CT	Alkane -CH2-	0.066	3.5	-0.12
CT	Alkane >CH-	0.066	3.5	0.205
OH	Alcohol -OH	0.17	3.12	-0.683
HC	Alkane H-C	0.03	2.5	0.06
HO	Alcohol -OH	0.0	0.0	0.418

Table S3: OPLS parameters: graphene and GO atom types

OPLS atom type	Description	Lennard-Jones parameters		Atomic charges		
		ϵ (Kcal mol^{-1})	σ (Å)			
CA	Aromatic C	0.07	3.55	0.0	-0.115	
HA	Aromatic H-C	0.03	2.42	0.115		
CT	Alcohol R3COH	0.066	3.5	0.2	0.265	
OH	Alcohol -OH	0.17	3.12	-0.683		
HO	Alcohol -OH	0.0	0.0	0.45	0.435	0.418
OS	Dialkyl Ether -O-	0.14	2.9	-0.4		
OH	Phenol -OH	0.17	3.07	-0.585		
C	Carboxylic Acid -COOH	0.105	3.75	0.635		
O	Carboxylic Acid C=O	0.21	2.96	-0.44		
OH	Carboxylic Acid -OH	0.17	3.0	-0.53		
CA	Phenol C-OH	0.07	3.55	0.15	-0.115	

Table S4: OPLS parameters: PVA Bonds

Atom types		Spring Constant (Kcal mol^{-1}/Å^2)	Equilibrium distance (Å)
CT	CT	268.0	1.529
CT	HC	340.0	1.09
CT	OH	320.0	1.41
OH	HO	553.0	0.945

Table S5: OPLS parameters: GO Bonds

Atom types		Spring Constant (Kcal mol^{-1}/Å^2)	Equilibrium distance (Å)
CA	CA	469.0	1.4
CA	CT	317.0	1.51
CT	CA	317.0	1.51
CT	CT	268.0	1.529
CA	HA	367.0	1.08
CA	C	400.0	1.49
CA	OH	450.0	1.364
C	O	570.0	1.229
C	OH	450.0	1.364
OH	HO	553.0	0.945
CT	OS	320.0	1.41
CT	OH	320.0	1.41

Table S6: OPLS parameters: PVA angles

Atom types			K (Kcal mol^{-1}/radian^2)	Equilibrium angle (degrees)
CT	CT	CT	58.35	112.7
CT	CT	HC	37.5	110.7
CT	CT	OH	50.0	109.5
CT	OH	HO	55.0	108.5
OH	CT	HC	35.0	109.5
HC	CT	HC	33.0	107.8

Table S7: OPLS parameters: GO angles

Atom types			K (Kcal mol^{-1}/radian^2)	Equilibrium angle (degrees)
OH	CA	CA	70.0	120.0
CA	CA	CA	63.0	120.0
CA	CA	HA	35.0	120.0
C	CA	CA	85.0	120.0
CA	CA	CT	70.0	120.0
CT	CA	CA	70.0	120.0
HA	CA	CT	35.0	117.0
OS	CT	CA	50.0	109.5
OS	CT	CT	50.0	109.5
CA	CT	CT	63.0	114.0
CA	CT	CA	40.0	109.5
CT	CT	CA	63.0	114.0
C	CA	CT	70.0	119.7
OH	CA	CT	70.0	124.0
CA	CT	OH	50.0	109.5
OH	CT	CA	50.0	109.5
CT	CA	CT	70.0	130.0
OH	CT	CT	50.0	109.5
CT	CT	CT	58.35	112.7
CA	CA	C	85.0	120.0
O	C	CA	80.0	120.4
O	C	OH	80.0	121.0
CA	C	OH	70.0	120.0
HO	OH	CA	35.0	113.0
C	OH	HO	35.0	113.0
CT	OS	CT	60.0	109.5
HO	OH	CT	55.0	108.5

Table S8: OPLS parameters: PVA dihedrals

Atom types				Kcal mol^{-1}			
				K_1	K_2	K_3	K_4
CT	CT	CT	CT	1.3	-0.05	0.2	0.0
CT	CT	CT	OH	-1.552	0.0	0.0	0.0
CT	CT	CT	HC	0.0	0.0	0.3	0.0
CT	CT	OH	HO	-0.356	-0.174	0.492	0.0
OH	CT	CT	HC	0.0	0.0	0.468	0.0
HC	CT	CT	HC	0.0	0.0	0.3	0.0
HC	CT	OH	HO	0.0	0.0	0.352	0.0

Table S9: OPLS parameters: GO dihedrals

Atom types				Kcal mol^{-1}			
				K_1	K_2	K_3	K_4
OH	CA	CA	CA	0.0	7.25	0.0	0.0
OH	CA	CA	HA	0.0	7.25	0.0	0.0
CA	CA	CA	CA	0.0	7.25	0.0	0.0
CA	CA	CA	HA	0.0	7.25	0.0	0.0
HA	CA	CA	CA	0.0	7.25	0.0	0.0
CA	CA	CA	C	0.0	7.25	0.0	0.0
C	CA	CA	CA	0.0	7.25	0.0	0.0
CA	CA	CA	OH	0.0	7.25	0.0	0.0
HA	CA	CA	CT	0.0	7.25	0.0	0.0
CA	CA	CA	CT	0.0	7.25	0.0	0.0
C	CA	CA	CT	0.0	7.25	0.0	0.0
CT	CA	CA	CT	0.0	7.25	0.0	0.0
CA	CA	CT	OS	0.0	0.0	0.0	0.0
CA	CA	CT	CT	0.0	0.0	0.0	0.0
CA	CA	CT	CA	0.0	0.0	0.0	0.0
HA	CA	CT	OS	0.0	0.0	0.468	0.0
HA	CA	CT	CT	0.0	0.0	0.468	0.0
HA	CA	CT	CA	0.0	-8.0	0.0	0.0
OS	CT	CA	C	0.5	0.0	0.0	0.0
OS	CT	CA	CA	0.0	0.0	0.0	0.0
CA	CT	CA	C	0.5	0.0	0.0	0.0
CA	CT	CA	CA	0.0	0.0	0.0	0.0
CT	CT	CA	C	0.5	0.0	0.0	0.0
CT	CT	CA	CA	0.0	0.0	0.0	0.0
CT	CA	CA	CA	0.0	7.25	0.0	0.0
CT	CA	CA	OH	0.0	7.25	0.0	0.0
OH	CA	CT	CT	0.0	0.0	0.468	0.0
OH	CA	CT	OS	0.0	0.0	0.468	0.0
OH	CA	CT	CA	0.0	-8.0	0.0	0.0
CA	CA	CT	OH	0.0	0.0	0.0	0.0
C	CA	CT	OH	0.5	0.0	0.0	0.0
CA	CT	CA	CT	0.0	-8.0	0.0	0.0
OH	CT	CA	OH	0.0	0.0	0.318	0.0
OH	CT	CA	CT	1.711	-0.5	0.663	0.0
CA	CT	CA	OH	0.0	-8.0	0.0	0.0
CT	CA	CT	OS	1.711	-0.5	0.663	0.0
CT	CA	CT	CT	2.817	-0.169	0.543	0.0
OS	CT	CA	CT	1.711	-0.5	0.663	0.0
CT	CT	CA	CT	2.817	-0.169	0.543	0.0
HA	CA	CT	OH	0.0	0.0	0.468	0.0
CT	CA	CT	CA	0.0	-8.0	0.0	0.0
CT	CA	CT	OH	1.711	-0.5	0.663	0.0
HA	CA	CA	HA	0.0	7.25	0.0	0.0
CA	CT	CT	CA	-4.344	-1.714	0.0	0.0
CA	CT	CT	CT	1.711	-0.5	0.663	0.0
CA	CT	CT	OS	-4.344	-1.714	0.0	0.0
OS	CT	CT	CT	1.3	-0.05	0.2	0.0
CT	CT	CT	CT	1.3	-0.05	0.2	0.0
CT	CT	CT	OH	-1.552	0.0	0.0	0.0
CA	CT	CT	OH	0.0	0.0	0.366	0.0
OS	CT	CT	OH	4.319	0.0	0.0	0.0
OS	CT	CT	OS	-0.55	0.0	0.0	0.0
OH	CT	CT	OH	9.508	0.0	0.0	0.0
CT	CT	CT	CA	1.711	-0.5	0.663	0.0
OS	CT	CT	CA	-4.344	-1.714	0.0	0.0
OH	CT	CA	CA	0.0	0.0	0.0	0.0
OH	CT	CT	CA	0.0	0.0	0.366	0.0
C	CA	CA	HA	0.0	7.25	0.0	0.0
OH	CA	CA	C	0.0	7.25	0.0	0.0
OH	CA	CA	CT	0.0	7.25	0.0	0.0
OH	CA	CA	OH	0.0	7.25	0.0	0.0
C	CA	CA	C	0.0	7.25	0.0	0.0
CA	CA	C	O	0.0	2.1	0.0	0.0
CA	CA	C	OH	0.0	2.1	0.0	0.0
CA	CA	OH	HO	0.0	1.682	0.0	0.0
CT	CA	C	O	0.9	0.23	-0.505	0.0
CT	CA	C	OH	0.9	0.23	-0.505	0.0
CT	CA	OH	HO	0.0	1.682	0.0	0.0
O	C	OH	HO	0.0	5.0	0.0	0.0
CA	C	OH	HO	4.0	5.0	0.0	0.0
CT	CT	OS	CT	0.65	-0.25	0.67	0.0
CA	CT	OS	CT	-0.521	-2.018	1.996	0.0
CT	CT	OH	HO	-0.356	-0.174	0.492	0.0
CA	CT	OH	HO	-0.9	0.0	0.0	0.0

Table S10: OPLS parameters: GO impropers

Atom types				K (Kcal mol^{-1}/radian^2)	Equilibrium angle (degrees)
CA	CA	CT	CA	5.0	180.0
CA	CT	CA	CA	5.0	180.0
CA	CA	CA	CT	5.0	180.0
CA	CA	HA	CT	5.0	180.0
CA	C	CT	CA	5.0	180.0
CA	OH	CA	CT	5.0	180.0
CA	CA	C	CT	5.0	180.0
CA	CA	CT	C	5.0	180.0
CA	CT	OH	CT	5.0	180.0
CA	HA	CT	CT	5.0	180.0
CA	CT	HA	CT	5.0	180.0
CA	CT	CA	OH	5.0	180.0
CA	CA	CT	HA	5.0	180.0
CA	HA	CT	CA	5.0	180.0
CA	CT	OH	CA	5.0	180.0
CA	CT	CA	HA	5.0	180.0
CA	CA	CT	OH	5.0	180.0
CA	C	CT	CT	5.0	180.0
CA	HA	CA	CT	5.0	180.0
CA	CA	OH	CT	5.0	180.0
CA	CT	HA	CA	5.0	180.0
CA	CT	CT	HA	5.0	180.0
CA	OH	CT	CA	5.0	180.0
CA	CT	CA	C	5.0	180.0
CA	CT	CT	OH	5.0	180.0
CA	C	CA	CT	5.0	180.0
CA	CT	C	CT	5.0	180.0
CA	CT	CT	CA	5.0	180.0
CA	CA	CT	CT	5.0	180.0
CA	CT	CT	CT	5.0	180.0
CA	CT	CA	CT	5.0	180.0
CA	OH	CT	CT	5.0	180.0
CA	CT	C	CA	5.0	180.0

References

(1) Sinclair, R. C. make-graphitics. `https://github.com/velocirobbie/make-graphitics`, 2020; Accessed: 2021-06-05.

(2) Sinclair, R. C.; Coveney, P. V. Modelling nanostructure in graphene oxide: inhomogeneity and the percolation threshold. *J. Chem. Inf. Model.* **2019**, *59*, 2741.

(3) Sinclair, R. C. make-graphitics. 2019; `https://doi.org/10.5281/zenodo.2548538`, `10.5281/zenodo.2548538`.

(4) Lerf, A.; He, H.; Forster, M.; Klinowski, J. Structure of Graphite Oxide Revisited. *J. Phys. Chem. B* **1998**, *102*, 4477–4482.

(5) Yang, J.; Shi, G.; Tu, Y.; Fang, H. High Correlation between Oxidation Loci on Graphene Oxide. *Angew. Chem. Int. Ed. Engl.* **2014**, *53*, 10190–10194.

(6) Groen, D.; Richardson, R. A.; Wright, D. W.; Jancauskas, V.; Sinclair, R.; Karlshoefer, P.; Vassaux, M.; Arabnejad, H.; Piontek, T.; Kopta, P., et al. Introducing VECMAtk-Verification, Validation and Uncertainty Quantification for Multiscale and HPC Simulations. 2019.